Experimental Determination of H_2 Solubilities in Liquid Fluorocarbons

Maria L. Japas, Chien-Ping Chai Kao, and Michael E. Paulaitis*

Department of Chemical Engineering, University of Delaware, Newark, Delaware 19716

An apparatus and experimental technique are described for measuring gas solubilities in liquids at elevated temperatures and pressures. The apparatus has been designed to operate at pressures up to 100 bar and temperatures up to 70 °C. The technique has been used to measure H_2 solubilities in perfluoropropane (C_3F_8) and perfluoropropylene (C_3F_6) at pressures up to 20 bar and temperatures from 0 to 50 °C. Two methods of regressing the experimental data to give Henry's law constants and for extrapolating gas solubilities beyond the experimental temperature range are also compared.

Experimental Technique

A stoichiometric experimental technique has been used to measure H_2 solubilities in liquid fluorocarbons at elevated pressures. The distinguishing feature of this technique is that compositions of the coexisting phases are calculated from a material balance; no sampling is required. This method has frequently been applied to studies of fluid-phase equilibria at elevated pressures and in the vicinity of critical points where sampling is both difficult and often the main source of experimental uncertainties (*1–3*). In these applications, vapor- and liquid-phase compositions are calculated from measurements of pressure as a function of the total volume of the system at constant temperature and overall composition.

A schematic representation of the experimental apparatus is shown in Figure 1. The apparatus consists of a high-pressure view cell, an injection system for loading known amounts of each component, and a pressurizing system for generating and measuring pressure in the cell. The high-pressure view cell is mounted on an aluminum C-frame which is placed in a constant-temperature bath. The bath temperature can be controlled to within 0.05 °C and is measured with a mercury thermometer to within 0.01 °C.

The view cell is a synthetic sapphire tube (Saphikon, Inc.) which facilitates determination of the number of coexisting phases and accurate measurement of the position of each phase boundary. The cell is sealed at both ends with neoprene O-rings mounted on stainless-steel endcaps. A movable piston separates the fluid under study in the equilibrium chamber of the view cell from the pressurizing fluid (water) in the remaining portion of the cell. The pressure in the equilibrium chamber is measured indirectly by measuring the water pressure with a strain gauge transducer calibrated to ±0.01 bar. The piston position can also be adjusted to vary the cell volume from 1 to 14 cm^3. The dynamic seals on this piston are spring-loaded Teflon seals (Bal Seal Co.) which require excess pressures of less than 0.1 bar to displace the piston.

The experimental procedure was as follows. Pure H_2 was injected into the evacuated equilibrium chamber, and the amount loaded was calculated from the measured pressure, temperature, and cell volume. Known amounts of fluorocarbon were then added with the syringe pump PG1 which had been precalibrated to determine the volume of liquid delivered as a function of pump displacement. After the system reached thermal equilibrium, the pressure was raised until the gas phase completely disappeared. Once the system was in the one-phase (liquid) region, the pressure was reduced incrementally while allowing the system to equilibrate after each step. The equilibrated volume at each step was recorded as a function of the measured pressure. A typical plot of piston displacement versus the change in pressure is shown in Figure 2. The transition from a single homogeneous liquid phase to two coexisting phases corresponding to gas–liquid equilibrium (i.e., the appearance of a gas bubble) can be observed visually during the experiment or more accurately obtained from the abrupt change in slope on the pressure–volume plot (point b in Figure 2).

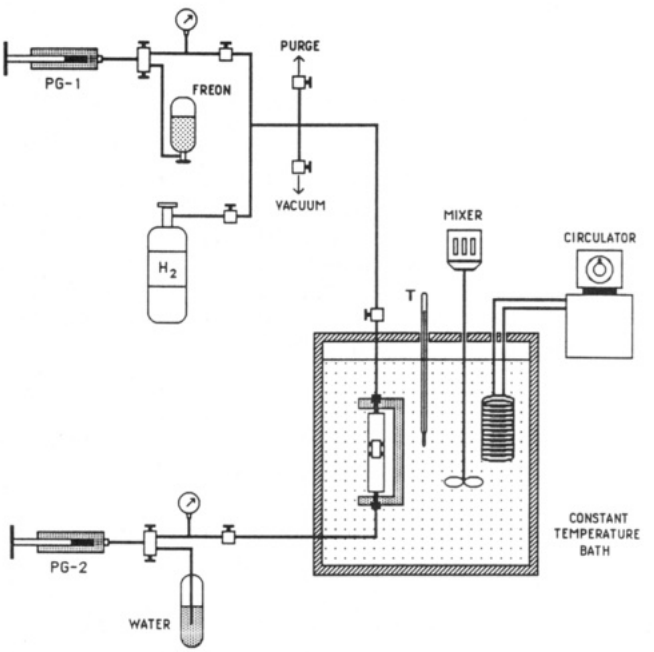

Figure 1. Schematic diagram of the experimental apparatus.

Data Analysis

Analysis of the experimental data relies on an accurate determination of the cell volume at the bubble point. This bubble-point volume provides a convenient reference point to enable an accurate determination of the gas-phase volume at each piston position as pressure is subsequently reduced within the two-phase region. The gas-phase volume and system pressure are the measured quantities required for calculating the gas-phase composition from which the liquid composition is obtained by a material balance. The gas solubility and Henry's constant are in turn obtained from this liquid composition. Corrections for thermodynamic nonidealities in the gas phase are computed using the Peng–Robinson equation of state (PR EOS) (*4*).

The measured quantities for each experiment are the constant temperature T, the number of moles of solvent n_1°

0021-9568/92/1737-0423$03.00/0

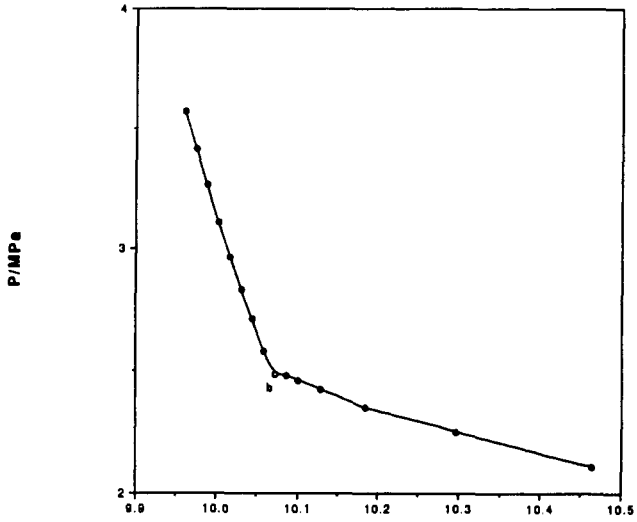

Figure 2. Measured system pressure vs total volume at constant temperature.

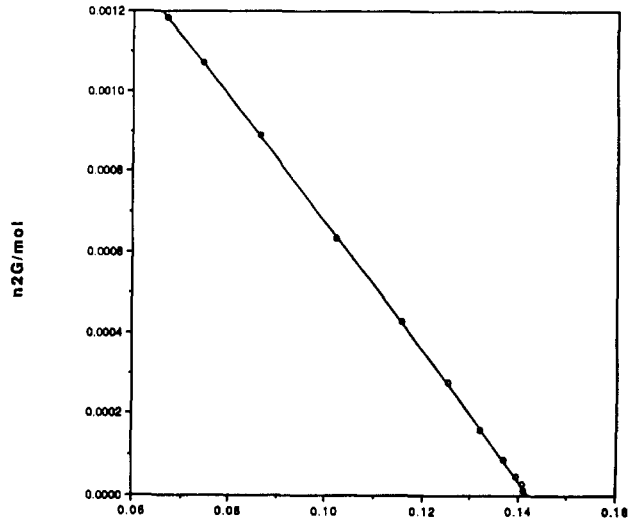

Figure 3. n_2^G vs $P_2\phi_2 n_1$.

and solute $n_2°$ loaded into the cell, the pressure P as a function of piston position l, and the piston position l_b and total pressure P_b at the bubble point. The experimental value of $n_2°$ was not considered to be accurate enough to use in the data analysis due to the likelihood of H_2 permeation through the Teflon seals. In the gas–liquid equilibrium region, the mole balance for H_2 (component 2) is

$$n_2° = n_2^L + n_2^G \tag{1}$$

where n_2^L and n_2^G are the number of moles of H_2 in the liquid and gas phases, respectively. Considering that

$$n_2^G = \frac{P_2 V^G}{Z^G RT} \tag{2}$$

where $P_2 = y_2 P$ (y_2 is the gas-phase mole fraction of H_2), Z^G is the compressibility factor for the gas phase, and V^G is the total volume of the gas phase and making the reasonable approximation

$$n_2^L \approx (P_2\phi_2/H_{2,1})n_1 \tag{3}$$

where ϕ_2 is the gas-phase fugacity coefficient for H_2 and $H_{2,1}$ is the Henry's law constant for H_2 in the liquid fluorocarbon, eq 1 can be rewritten as

$$n_2^G = P_2 V^G/Z^G RT = n_2° - P_2\phi_2 n_1/H_{2,1} \tag{4}$$

Equation 4 shows that a plot of n_2^G versus $P_2\phi_2 n_1$ should give a straight line, and the slope of this line will yield Henry's constant, $H_{2,1}$. The analysis requires values of Z^G, y_2, and ϕ_2 for the gas mixture. These quantities can be calculated from the PR EOS as outlined in Appendix A.

The total volume of the gas phase, V^G, is obtained from the difference between l and l_b, and the calibrated cross-sectional area of the sapphire tube. Three corrections to V^G were considered: (1) a decrease in liquid volume due to evaporation of solvent as V^G is increased ($=n_1^G v_1^L$); (2) a decrease in liquid volume due to evaporation of H_2 as V^G is increased or as P_2 is decreased ($=n_2^G v_2^L$); (3) an increase in liquid volume as the total pressure is decreased due to the compressibility of the liquid phase ($=\kappa_T(P - P_b)v^L$). The last two corrections have opposite signs and are similar in magnitude, and thus cancel each other within the experimental uncertaintiy of the measured gas volumes (5 mm³). Consequently, only the first correction is taken into account to give the following expression for the total volume of the gas phase:

$$V^G \approx \frac{A(l - l_b)}{(1 - Z^L/Z^G)} \tag{5}$$

where Z^L is the compressibility factor for the pure liquid fluorocarbon at its saturation pressure, and is evaluated using the PR EOS. In all cases, the ratio Z^L/Z^G was found to be small, corresponding to a correction of less than 5% of the total gas volume. A typical plot of n_2^G versus $P_2\phi_2 n_1$ is shown in Figure 3. For all conditions studied, n_2^G was found to be a linear function of $P_2\phi_2 n_1$ to within a standard deviation of approximately 1% or less. The overall experimental uncertainty in $H_{2,1}$ determined from the slope of these plots is estimated to be approximately 2%.

In addition to Henry's constant, the infinite-dilution distribution coefficient for H_2 was calculated from

$$K_D = \lim_{x,y\to 0} y/x = H_{21}/P_1^{sat}\phi_2^{\infty} \tag{6}$$

where P_1^{sat} is the vapor pressure of the pure fluorocarbon at saturation, and ϕ_2^{∞} is the fugacity coefficient for H_2 at infinite dilution in the gas mixture at P_1^{sat}.

An alternative approach to analyzing the experimental data was also investigated. This approach consists of the direct application of the PR EOS to calculate gas–liquid equilibrium, from which liquid compositions are obtained as an iterative solution to the following material balance equations:

$$n_i^G = y_i V^G/v^G \tag{7}$$

$$n_i^L = n_i° - n_i^G \tag{8}$$

$$x_i = n_i^L/(n_1^L + n_2^L) \tag{9}$$

where v^G is the vapor molar volume, and the subscripts refer to either component in the mixture.

The mixing rules in the PR EOS contain two interaction parameters for each pair of mixture constituents: δ_{ij} and η_{ij} (see Appendix A). For both H_2/fluorocarbon mixtures, η_{12} is set to −0.1, while δ_{12} and the total amount of hydrogen loaded into the cell, $n_2°$, are adjusted to minimize the root mean square deviation of measured and calculated pressures. The Henry's law constant is computed from its definition:

$$H_{2,1} = (f_2^L/x_2)_{x_2\to 0, P\to P_1^{sat}} \tag{10}$$

Table I. Experimental Values of Henry's Constants $H_{2,1}$ and Infinite-Dilution Distribution Coefficients $T \log K_D$

T/K	$H_{2,1}$/MPa	ρ_1/(mol dm^{-3})	(T/K) log K_D
	C_3F_6 (1) + H_2 (2) (ρ_c = 3.241 mol dm^{-3})		
278.40	82.3	9.375	631
304.01	65.5	8.564	543
	C_3F_8 (1) + H_2 (2) (ρ_c = 3.340 mol dm^{-3})		
275.87	62.1	7.642	574
298.16	47.6	7.034	493
322.11	32.3	6.135	381

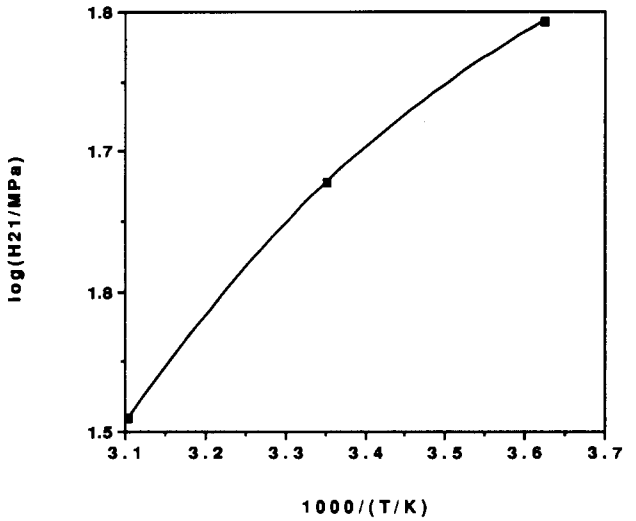

Figure 4. Temperature dependence of $H_{2,1}$ for H_2 in C_3F_8.

where f_2^L is the fugacity of hydrogen in the liquid phase, calculated directly from the PR EOS.

Results

As a check of the stoichiometric technique, the solubility of H_2 in CCl_2FCClF_2 (FC113) was measured at 29.10 °C and compared to the literature value. Corrections for gas-phase nonidealities are small for this system, since the vapor pressure for the fluorocarbon is relatively low. These corrections were made using the virial equation of state and fluorocarbon properties (i.e., virial coefficients, liquid density, and vapor pressure) taken from the literature (5). A value of 151 MPa was obtained for Henry's constant at this temperature, which is in good agreement with the literature value of 148 MPa (6).

The experimental values of $H_{2,1}$ are given in Table I. A comparison of Henry's constant for the saturated fluorocarbon (C_3F_8) to those for the unsaturated fluorocarbon (C_3F_6) shows higher H_2 solubilities in the saturated fluorocarbon. Henry's constants for H_2 solubilities in C_3F_8 are also plotted as a function of temperature in Figure 4 and show that the partial molar enthalpy of H_2 dissolution in C_3F_8 increases with increasing temperature. It has been observed that the partial molar enthalpy of dissolution for a dilute, volatile solute is a strong function of temperature, and indeed diverges at the critical point of the solvent (8). Thus, simple extrapolations in temperature of Henry's constants beyond the temperature range investigated cannot be accomplished with a high degree of confidence. A plot of $T \log K_D$ versus the saturated liquid density of the pure solvent will, however, give a straight line over almost the entire range of saturated liquid densities (9, 10). Moreover, reliable extrapolations to high temperatures can be performed since, by definition, the value of K_D at the critical point of the solvent is equal to unity, and the quantity $T \log K_D$ should be identically zero at this point. This method of extrapolating gas solubilities to higher temperatures was tested by plotting the experimental values of $T \log K_D$ from Table I versus the difference in the saturated liquid density and critical density of the pure solvent. The critical densities for both fluorocarbons are also given in Table I. The results are plotted in Figure 5 and show that linear extrapolations of the experimental $T \log K_D$ values to the critical point of the solvent are justifiable and give reasonable estimates for the critical densities of the two fluorocarbons. The extrapolated critical density for C_3F_6 is 10% higher than the value given in Table I, and for C_3F_8, this value is 5.4% lower than that given in Table I. These discrepancies may in fact be

Table II. Henry's Constants $H_{2,1}$ Obtained from Different Data Regressions for C_3F_6 (1) + H_2 (2)

T/°C	$H_{2,1}^{exp}$/atm	$H_{2,1}^{PR}$/atm	δ_{12}
5.25	812	827	0.054
30.86	646	668	0.186

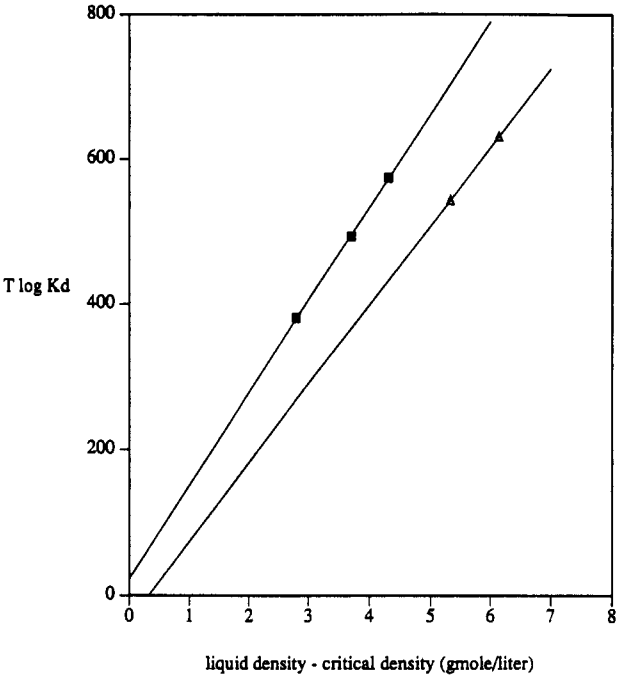

Figure 5. $T \log K_D$ vs liquid density: hydrogen solubility in fluorocarbons.

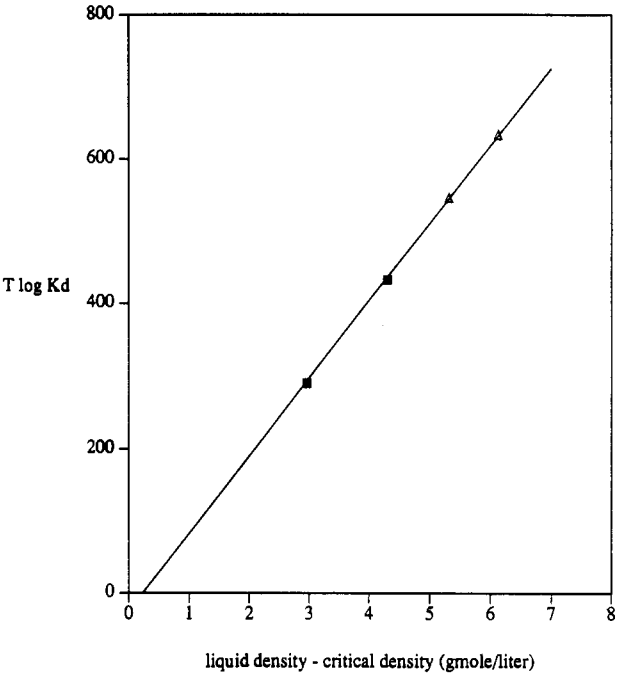

Figure 6. $T \log K_D$ vs liquid density for H_2 in C_3F_6: hydrogen (1) + FC1216 (2).

due to uncertainties in the estimated critical densities for the fluorocarbons, which were obtained from saturated vapor and liquid densities along the gas–liquid coexistence curve using the law of rectilinear diameters (7).

Henry's constants, $H_{2,1}^{PR}$, obtained from direct application of the PR EOS to regress the experimental data, are compared with the experimental values in Table II for $H_2 + C_3F_6$. The differences in Henry's constants are not large: 1.8% at 5.25 °C and 3.4% at 30.86 °C. The last column in Table II also gives the regressed value of the PR EOS interaction parameter, δ_{ij}, which is found to have a significant temperature dependence. If we make the reasonable assumption that this parameter varies linearly with temperature, the extrapolation of $T \log K_D$ values in Figure 5 can alternatively be accomplished on the basis of PR EOS calculations. The results are shown in Figure 6 where the two solid squares represent the PR EOS calculations with δ_{ij} linearly dependent on temperature and the two open triangles represent the experimental $T \log K_D$ values. The four points can be fit to a straight line which, when extrapolated to $T \log K_D = 0$, gives a critical density for C_3F_6 that is only 7% higher than the value in Table I. However, the extrapolated value of δ_{ij} at the highest temperature is 0.42 which is too large to be physically meaningful. We therefore conclude that the two methods of regressing the experimental data yield nearly identical results for Henry's constants and provide for reasonable extrapolations of the solubility data to higher temperatures. However, the basis for this extrapolation with either method is largely empirical.

Appendix A. PR EOS Calculations of Gas-Phase Thermodynamic Properties

Deviations from ideal gas behavior were calculated using the Peng–Robinson equation of state with parameters for H_2 taken from the original work of Peng and Robinson (4) and the corresponding parameters for the fluorocarbons obtained from Sweany (7). The following iterative procedure was used (component 1, fluorocarbon; component 2, H_2).

(1) An initial guess for the gas-phase composition, y_2, was made.

(2) The PR EOS parameters for the gas mixture were calculated from this initial guess using conventional mixing rules

$$a_m = \sum_{i,j} y_i y_j a_{ij} \tag{A1}$$

$$b_m = \sum_{i,j} y_i y_j b_{ij} \tag{A2}$$

with the geometric mean combining rule for a_{ij}

$$a_{ij} = a_{ji} = (1 - \delta_{ij})(a_{ii} a_{jj})^{1/2} \tag{A3}$$

and the arithmetic mean combining rule for b_{ij}

$$b_{ij} = b_{ji} = (1 - \eta_{ij})(b_{ii} + b_{jj})/2 \tag{A4}$$

where $\delta_{ii} = \eta_{ii} = 0$.

(3) The PR EOS was solved to find the root corresponding to the gas-phase volume.

(4) The gas-phase fluorocarbon fugacity at the temperature and pressure of interest was calculated.

(5) The gas-phase composition was recalculated by equating gas- and liquid-phase fugacities for the fluorocarbon, assuming that the liquid phase is dilute in solute 2 (i.e., $\gamma_1 = 1$).

$$y_1 = 1 - y_2 = \frac{x_1 P_1^{sat} \phi_1^{sat}}{\phi_1 P} \exp\left[\frac{v_1 (P - P_1^{sat})}{RT}\right] \tag{A5}$$

This assumption is reasonable since x_1 was found to be greater than 0.97 in all cases.

(6) The new gas-phase composition was then compared to the initial guess, and steps 2–5 were repeated until successive gas-phase mole fractions converged to within $\pm 10^{-4}$. The gas-phase molar volume, compressibility factor, and component fugacity coefficients corresponding to this composition were then calculated.

Literature Cited

(1) DiAndreth, J. R.; Ritter, J. M.; Paulaitis, M. E. *Ind. Eng. Chem. Res.* **1987**, *26*, 337.
(2) Ritter, J. M.; Palavra, A. M. F.; Chai Kao, C.-P.; Paulaitis, M. E. *Fluid Phase Equilib.* **1990**, *55*, 173.
(3) Crovetto, R.; Fernandez Prini, R.; Japas, M. L. *Ber. Bunsen-Ges. Phys. Chem.* **1984**, *88*, 484.
(4) Peng, D. Y.; Robinson, D. B. *Ind. Eng. Chem. Fundam.* **1976**, *15*, 59.
(5) Smith, B. D.; Srivastava, R. *Thermodynamic Data for Pure Compounds. Part B. Halogenated Hydrocarbons and Alcohols*; Elsevier: New York, 1986.
(6) Young, C. L. *Solubility Data Series*; Pergamon Press: Oxford, 1981; Vols. 5, 6.
(7) Sweany, G. A., E. I. du Pont de Nemours & Co., Inc. Personal communication, 1991.
(8) Chang, R. F.; Morrison, G.; Levelt Sengers, J. M. H. *J. Phys. Chem.* **1984**, *88*, 3389.
(9) Japas, M. L.; Levelt Sengers, J. M. H. *AIChE J.* **1989**, *35*, 705.
(10) Harvey, A. H.; Crovetto, R.; Levelt Sengers, J. M. H. *AIChE J.* **1990**, *36*, 1901.

Received for review March 3, 1992. Accepted May 26, 1992.

Registry No. H_2, 1333-74-0; C_3F_8, 76-19-7; C_3F_6, 116-15-4.